ORIGINAL PAPER

The effect of pressure gradient on anode micro modeling of solid oxide fuel cell

Aosheng Hu · Jianqiu Zhou · Bingbing Chen · Youyi Wu

Abstract A theoretical mathematical model is established to investigate the effect of pressure gradient on electrochemical characteristics of anode in solid oxide fuel cell (SOFC) running on pre-reformed methane fuel. The model adopts micro modeling approach in which anode is treated as porous composite structure of electronic and ionic conducting particles. It includes mass conservation, mass transfer, chemical and electrochemical reactions, and charges transfer. Besides, the electrochemical characteristics of anode have been discussed with and without pressure gradient in the dusty-gas model. It can be found that the pressure increases along the anode depth. The molar fractions of fuel species are different under the consideration of pressure gradient. The results revealed by the developed model verify the point of treating a SOFC electrode as two finite layers. Only in the reaction zone layer, the pressure gradient can obviously influence electronic and ionic current densities, electronic and ionic potentials, and anode activation overpotential.

Keywords Solid oxide fuel cell · Micro modeling · Pressure gradient · Two finite layers · Mass transfer

Introduction

Solid oxide fuel cell (SOFC) is a solid-state ceramic cell, which has received more and more extensive attention for use in the direct conversion of chemical energy of fuel into electricity and heat due to its low pollutant emissions, high energy efficiency, fuel flexibility, and co-generation units power generation in both large central power plants and decentralized generation facilities in the future [1].

Among various configurations in which SOFC exists, two common ones are tubular and planar SOFC. Because of higher power density and simplicity in manufacturing, the planar-type design of SOFC has received more and more attention lately [2, 3]. Although significant progress has been made for the tubular-type configuration of SOFC, this type of SOFC has lower power density due to high electrical resistance caused by long current paths [3]. In contrast, the planar-type configuration of SOFC is capable of achieving higher power density [3, 4]. Besides, anode-supported configurations in the planar-type SOFCs are usually considered to be superior to electrolyte/cathode-supported ones [5–8] and chosen as the model configurations.

When SOFC is operating at high temperature (1,073–1,273 K), it has a number of advantages over low-temperature fuel cell: (1) the electrolyte has a higher ionic conductivity at high temperature, then ohmic overpotential of electrolyte can be minimized; (2) the electrochemical reactions are rapid at high temperature, leading to low activation overpotential and effective utilization of low cost catalyst, for instance, Ni; and (3) direct internal reforming of hydrocarbon fuels can be occurred in SOFC because of high operating temperature, hence, a variety of fuels can be utilized, such as H_2, CH_4, C_2H_6, C_3H_8, and so on. What is more, CO also can be used, which is an unwished poisonous gas for low-temperature fuel cells, such as phosphoric acid fuel cell; (4) waste heat from SOFC is high-quality and can be recycled by using a bottoming cycle to increase the system efficiency [9].

Whereas, the commercialization of planar-type SOFC has some technical questions due to its high temperature. For example, disadvantageous thermal expansion mismatch of SOFC components, internal stresses in cell components

A. Hu · J. Zhou (✉) · B. Chen · Y. Wu
School of Mechanical and Power Engineering, Nanjing Tech University, Nanjing, Jiangsu Province 210009, China
e-mail: zhouj@njtech.edu.cn

caused by thermal shocks, or heat cycles and catalyst sintering. Therefore, it is vital to reduce operating temperature to an intermediate range (823–1,073 K), usually known as intermediate-temperature SOFC [10].

Generally, SOFC anode is made of cermet of Ni/YSZ (Nickel and YSZ, yttria stabilized zirconia), electrolyte consists of YSZ (yttria stabilized zirconia), and cathode is composed by electron-conducting electrocatalytic material (LSM, strontium-doped lanthanum manganate) [11].

In the past few years, numerous models of SOFC exist in the literatures [11–21]. The models can be categorized into macro models [12–14, 16] and micro models [11, 15, 17, 22–24] depending on the treatment of electrode. For macro modeling, the electrode is treated as porous structure of electronic conducting particles along with electrochemical reaction considered to occur exclusively at the electrode/electrolyte interface. Most of them have not taken into account the effect of pressure gradient. However, the pressure gradient has been discussed in the anode macro modeling of a SOFC running on hydrocarbon fuels in literature from Ni et al. [16]. For micro modeling, the electrode is treated as porous structure of electronic and ionic conducting particles with electrochemical reaction considered to occur throughout the electrode. In literature for micro-scale modeling, the properties of porous electrodes and their effects on SOFC performance have been studied from different aspects [15, 25–28]. However, none of them take into account the role of pressure gradient during the process of mass transport which means the pressure is constant, whereas the pressure gradient exists in SOFC where the pre-reformed methane is used [16]. It is still not understand how and to what extent the existence of pressure gradient affects the electrochemical characteristics of anode in micro modeling. The study of the influence of pressure gradient in micro modeling is necessary. Thus, taking the micro modeling as an example, the object of this study is to numerically investigate whether the pressure gradient can influence the electrochemical characteristics of anode by micro modeling approach.

In this paper, the pre-reformed methane is employed for SOFC. Unlike other previous researches on micro modeling, the change of pressure in the pore is considered ($dP/dx \neq 0$). A dusty-gas model (DGM) that takes into account the diffusion and pressure gradient throughout the anode will be applied to describe the multi-component diffuse through the anode. This work aims to study the effect of pressure gradient on the electrochemical characteristics of anode. How the pressure varies along the anode depth is investigated; how the pressure gradient affects the molar fractions of species, the MSR reaction rate, electronic and ionic current densities, electronic and ionic potentials, and anode activation overpotential is also considered. The results can verify the concept of considering a SOFC electrode as two finite layers [11] as well. Therefore, a more accurate model can be proposed to predict and optimize the SOFC anode performance.

## Description of mathematical model

The geometry and principle of composite anode

The configurations of unit SOFC with single channel and its two dimensional cross section can be simply described in Fig. 1. Figure 2 shows the scheme of a SOFC composite anode. The coupled models considering electrochemical oxidation reactions, chemical reactions, mass transfer, and charge transfer in composite anode will be described later. In most studies [12, 14, 29–31], H_2 is usually used as fuel for SOFC, but SOFC also can be fed with hydrocarbon fuels, such as pre-reformed methane. In this study, pre-reformed methane is used as the fuel which consists of CH_4, CO, CO_2, H_2, and H_2O. In addition, it is assumed that the reactant gas mixtures are approximated as ideal gases with negligible Dofour, Soret, and gravity effects. The main chemical reactions involved are methane steam reforming reaction (MSR) and water gas shift reaction (WGS), given as follows:

$$CH_4 + H_2O \leftrightarrow CO + 3H_2 (\text{MSR}) \tag{1}$$

$$CO + H_2O \leftrightarrow CO_2 + H_2 (\text{WGS}) \tag{2}$$

When the SOFC is working, the transfer and reaction processes in composite anode can be summarized as: (1) the fuel transports from the anode surface to the active sites through the void space accompanies with methane steam reforming reaction and water gas shift reaction; (2) electrochemical oxidation reaction of H_2 and O^{2-} to form H_2O and electrons at the active sites; (3) transport of O^{2-} from the electrolyte to the active sites through the ion-conducting particles in the composite anode; and (4) transport of electrons from the active sites to current collector through the electron-conducting particles and transport of H_2O from the active sites to the anode surface through the void space in the composite anode. From process (2), it can be seen that only H_2 takes part in the electrochemical oxidation reaction. It should be noted that both H_2 and CO could be electrochemically oxidized at the three phrase boundaries (TPBs) where the electrochemical reactions are most active. However, it is reasonable to neglect the electrochemical oxidation of CO, because: (1) The rate of CO electrochemical oxidation is much lower than the electrochemical oxidation of H_2; (2) The rate of CO electrochemical oxidation is much lower than the chemical oxidation of CO by

Fig. 1 **a** Structure of unit cell with single channel. **b** Cross section A-A of unit cell
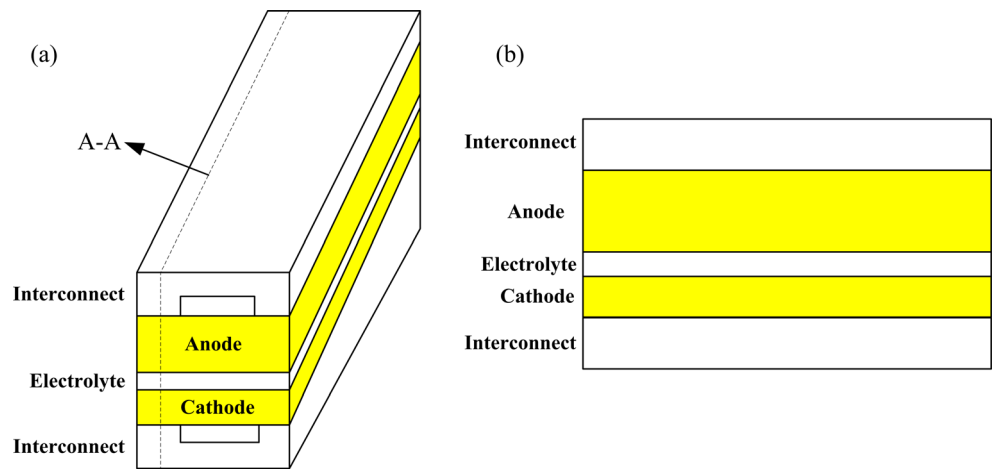
WGS [32, 33]. Electrochemical oxidation reaction of H_2 can be described as:

$$H_2 + O^{2-} \leftrightarrow H_2O + 2e^{-1} \tag{3}$$

The packed spherical shaped particles inside composite anode form the void space, tortuous flow paths and interfacial surface between ionic and electronic conducting particles. The composite anode is assumed to operate under steady state, zero stress condition, without consideration of NiO to Ni conversion and the parameters change only in the x direction, shown in Fig. 2. Also, temperature is assumed to be uniform throughout the whole anode. Suwanwarangkul et al. [31] concluded that DGM is the most appropriate model to simulate gas transport phenomena inside SOFC electrode.

The mathematical model describing the processes in composite anode is established by applying conservation equations of gas species along with the DGM for multicomponent gas diffusion, conservation equations of electronic and ionic charge. The governing equations are described in the following sections.
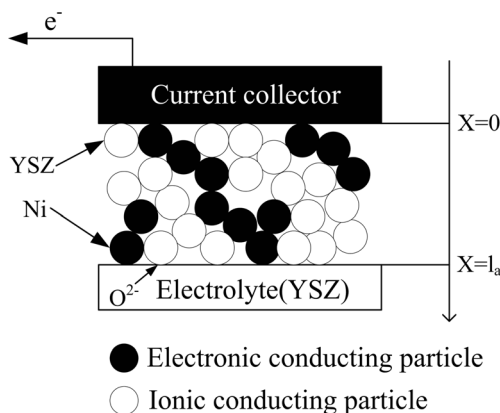

Fig. 2 Scheme of a SOFC composite anode

The model of mass conservation

The mass conservation equation in composite anode for each component can be written as:

$$\frac{\varepsilon}{RT}\frac{\partial(y_iP)}{\partial t} = -\nabla \cdot N_i + \dot{S}_{s,i} \tag{4}$$

The term on the left hand side vanishes under steady state condition. Then Eq. (4) can be simplified as:

$$\nabla \cdot N_i = \dot{S}_{s,i} \tag{5}$$

Where N_i (mol/(m² s)) is the molar flux of species i; P(Pa) is the total pressure throughout the anode; y_i is the molar fraction of species i; T(K) is the absolute temperature; R(8.3143 J/(mol K)) is universal gas constant; $\dot{S}_{s,i}$ (mol/(m³ s)) is the species source terms representing the rate of production or consumption of species due to MSR, WGS and H_2 electrochemical oxidation reaction in the anode; ε is the porosity.

From the literature [34], different expressions of reaction rate can be found. The expression of reaction rate averaged to per unit volume for a planar anode-supported SOFC from Lehnert et al. [35] is used in this study, as:

$$r_{\text{MSR}} = k_{MSR}^+ p_{CH_4} p_{H_2O} - k_{MSR}^- p_{CO} p_{H_2}^3 \tag{6}$$

$$r_{\text{WGS}} = k_{WGS}^+ p_{CO} p_{H_2O} - k_{WGS}^- p_{CO_2} p_{H_2} \tag{7}$$

Where p_i(Pa) is the partial pressure of species i; k_{MSR}^+ (mol/(m³ Pa² s)), k_{MSR}^- (mol/(m³ Pa⁴ s)), k_{WGS}^+ (mol/(m³ Pa² s)), and k_{WGS}^- (mol/(m³ Pa² s)) are rate constants;

the superscripts "+" and "−" refer to the forward and backward reactions, respectively; and $r_{MSR}(mol/(m^3 s))$ and $r_{WGS}(mol/(m^3 s))$ are the volumetric reaction rates for the methane steam reforming reaction and water gas shift reaction, respectively.

In terms of molar fractions, Eq. 6 and 7 can be written as:

$$r_{MSR} = P^2\left(k_{MSR}^+ y_{CH_4} y_{H_2O} - P^2 k_{MSR}^- y_{CO} y_{H_2}^3\right) \tag{8}$$

$$r_{WGS} = P^2\left(k_{WGS}^+ y_{CO} y_{H_2O} - k_{WGS}^- y_{CO_2} y_{H_2}^3\right) \tag{9}$$

In order to calculate rate constants, the equilibrium constants K_p are introduced, which can be determined from the following empirical relations [36] for the MSR and WGS, as:

$$K_{p,MSR} = \frac{k_{MSR}^+}{k_{MSR}^-} = 1.0267 \times 10^{10}$$
$$\times \exp\left(-0.2531\xi^4 + 0.3665\xi^3 + 0.5810\xi^2 - 27.134\xi\right) + 3.2770\right)(Pa^2) \tag{10}$$

$$K_{p,WGS} = \frac{k_{WGS}^+}{k_{WGS}^-}$$
$$= \exp\left(-0.2935\xi^3 + 0.6351\xi^2 + 4.1788\xi + 0.3169\right) \tag{11}$$

Where $\xi = \frac{1000}{T(K)-1}$

The forward reaction rate constants for the MSR and WGS can be described as [36]:

$$k_{MSR}^+ = 2395\exp\left(-\frac{231266}{RT}\right) \tag{12}$$

$$k_{WGS}^+ = 0.0171\exp\left(-\frac{103191}{RT}\right) \tag{13}$$

From Eqs. 10 to 13, we can obtain the forward reaction rate constants and equilibrium constants for the methane steam reforming reaction and water gas shift reaction. Hence, the backward reaction rate constants can be calculated by using equalities in Eqs. 10 and 11.

Therefore, the species source terms in the composite anode due to MSR and WGS can be described as:

$$\dot{S}'_{s,1} = -r_{MSR} \tag{14}$$

$$\dot{S}'_{s,2} = r_{WGS} \tag{15}$$

$$\dot{S}'_{s,3} = r_{MSR} - r_{WGS} \tag{16}$$

$$\dot{S}'_{s,4} = -r_{MSR} - r_{WGS} \tag{17}$$

$$\dot{S}'_{s,5} = 3r_{MSR} + r_{WGS} \tag{18}$$

Where 1 to 5 are CH_4, CO_2, CO, H_2O, and H_2, respectively. The numbers denote the same meaning in the sections blow.

The species source terms in the composite anode due to electrochemical oxidation of H_2 is related to volumetric current density produced through the Faraday's law of electrochemical oxidation reaction and is described as:

$$\dot{S}''_{s,i} = -\frac{\nu_i R_a}{n_e F} \tag{19}$$

where n_e is the amount of electrons participating in the electrochemical oxidation reaction; F(96,487 C/mol) is the Faraday's constant; and ν_i is the stoichiometric coefficient of species i involved in the oxidation reaction expressed in the following form:

$$H_2 + O^{2-} - H_2O \leftrightarrow 2e^{-1} \tag{20}$$

Besides, R_a(A/m^3) is the volumetric current density produced in the anode, which can be given by the general Butler-Volmer equation:

$$R_a = A_v i_{0,ref}^{H_2}\left(\frac{c_{H_2}}{c_{H_2,ref}}\right)^{\gamma_{H_2}}$$
$$\left\{\exp\left[\frac{\beta n_e F(\phi_i - \phi_e)}{RT}\right] - \exp\left[-\frac{(1-\beta)n_e F(\phi_i - \phi_e)}{RT}\right]\right\} \tag{21}$$

where A_v(m^2/m^3) is the actual reactive surface area per unit volume; $i_{0,ref}^{H_2}$ (A/m^2) is the reference exchange current density for hydrogen electrochemical oxidation reaction at reference hydrogen concentration $c_{H_2,ref}$ (mol/m^3); β is the charge transfer coefficient, whose value lies between zero and one, here β=0.5; ϕ_i (V) is the ionic potential; ϕ_e (V) is the electronic potential; and γ_{H_2} is the reaction order for H_2 oxidation.

For incorporating micro structural effects into the model to enhance its predictive ability, the expression used to model the reactive surface area per unit volume is provided by Costamagna et al. [25]:

$$A_v = \pi \sin^2 \theta r_{el}^2 n_t n_{el} n_{io} \frac{Z_{el} Z_{io}}{Z} \chi_{el} \chi_{io} \tag{22}$$

Where θ is the contact angle between the electronic and ionic conducting particles in the anode, as shown in Fig. 3; n_t is the total number of particles per unit volume; n_{el} and n_{io} are the number fractions of the electronic and ionic conducting particles in the anode, respectively; Z_{el} and Z_{io} are the coordination numbers of the electronic and ionic conducting particles in the anode, respectively; Z is the total average number of contacts of each particle; χ_{el} and χ_{io} are the probabilities of the electronic and ionic conducting particles in the anode, respectively.

The parameters required to obtain the reactive surface area per unit volume are calculated by adopting the following expressions [25, 37]:

$$n_t = \frac{1-\varepsilon}{\frac{4}{3} \pi r_{el}^3 \left[n_{el} + (1-n_{el}) \left(\frac{r_{io}}{r_{el}} \right)^3 \right]} \tag{23}$$

$$n_{el} = \frac{\Phi}{\left[\Phi + \frac{1-\Phi}{\left(\frac{r_{io}}{r_{el}} \right)^3} \right]} \tag{24}$$

$$Z_{el} = 3 + \frac{Z-3}{\left[n_{el} + (1-n_{el}) \left(\frac{r_{io}}{r_{el}} \right)^2 \right]} \tag{25}$$

$$Z_{io} = 3 + \frac{(Z-3) \left(\frac{r_{io}}{r_{el}} \right)^2}{\left[n_{el} + (1-n_{el}) \left(\frac{r_{io}}{r_{el}} \right)^2 \right]} \tag{26}$$

● Electronic conductor   ○ Ionic conductor

Fig. 3 Scheme of particles contact

where Φ is the volume fraction of the electron-conducting particles in the anode; Z is the total average coordination number, equal to 6 [37].

$$\chi_{el} = \left[1 - (2 - Z_{el-el}/2)^{2.5} \right]^{0.4} \tag{27}$$

$$\chi_{io} = \left[1 - (2 - Z_{io-io}/2)^{2.5} \right]^{0.4} \tag{28}$$

Where

$$Z_{el-el} = \frac{n_{el} Z_{el}^2}{Z} \tag{29}$$

$$Z_{io-io} = \frac{n_{io} Z_{io}^2}{Z} \tag{30}$$

From the above description, the species source terms in composite anode can be expressed as follows:

$$\dot{S}_{s,i} = \dot{S}'_{s,i} + \dot{S}''_{s,i} \tag{31}$$

That is:

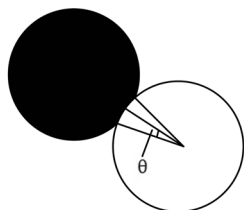$$\dot{S}_{s,1} = -r_{MSR} \tag{32}$$

$$\dot{S}_{s,2} = r_{WGS} \tag{33}$$

$$\dot{S}_{s,3} = r_{MSR} - r_{WGS} \tag{34}$$

$$\dot{S}_{s,4} = -r_{MSR} - r_{WGS} + \frac{R_a}{n_e F} \tag{35}$$

$$\dot{S}_{s,5} = 3 r_{MSR} + r_{WGS} - \frac{R_a}{n_e F} \tag{36}$$

The model of mass transfer

There are different multi-component diffusion models in chemical engineering literatures, for instance, the Fick's model (FM), Stefan-Maxwell model (SMM), DGM, etc. Both FM and DGM use mass transport equations taking into account Knudsen diffusion, molecular diffusion and the effect of pressure gradient. FM and DGM are used to describe the transport of components within porous media while SMM is a well-known mass transport model applied to nonporous media.

Ionics (2015) 21:2005–2017

The FM, the oldest approach to predict the diffusion, is applicable for binary mixtures or dilute solutions but not for multi-component mixtures. The SMM does not consider the collision of the gas molecules with the pore walls which is known as Knudsen diffusion and cannot accurately describe gas diffusion in porous media. Therefore, FM and SMM are not discussed further in this study, DGM is adopted. DGM takes into account the molecular diffusion, Knudsen diffusion, and a finite pressure gradient for the multi-component mass transfer in the porous electrodes, given as:

$$
\frac{N_i}{D_{i,k}^{eff}} + \sum_{j=1,j\neq i}^{n} \frac{y_j N_i - y_i N_j}{D_{ij}^{eff}}
$$
$$
= -\frac{1}{RT}\left[P\frac{dy_i}{dx} + y_i\frac{dP}{dx}\left(1 + \frac{B_0 P}{D_{i,k}^{eff}\mu_m}\right)\right] \tag{37}
$$

If the effect of pressure gradient is neglected, then Eq. 37 is simplified to:

$$
\frac{N_i}{D_{i,k}^{eff}} + \sum_{j=1,j\neq i}^{n} \frac{y_j N_i - y_i N_j}{D_{ij}^{eff}} = -\frac{P}{RT}\frac{dy_i}{dx} \tag{38}
$$

Summation over the index i for Eq. 37, the second term on the left hand side goes to zero, it can reach the pressure gradient term:

$$
\nabla P = -\frac{RT\sum\limits_{i=1}^{n}\dfrac{N_i}{D_{ij}^{eff}}}{1 + \sum\limits_{i=1}^{n}\dfrac{y_i B_0 P}{\mu_m D_{i,k}^{eff}}} \tag{39}
$$

Taking Eq. 39 into 37, and rearranging Eq. 37:

$$
\nabla y_i = \left(\frac{RT}{P}\right)\left[\sum_{j=1,j\neq i}^{n} \frac{y_i N_j - y_j N_i}{D_{ij}^{eff}} - \frac{N_i}{D_{i,k}^{eff}} - \frac{y_i}{RT}\left(1 + \frac{B_0 P}{\mu_m D_{i,k}^{eff}}\right)\nabla P\right] \tag{40}
$$

Where y_i and $D_{i,k}^{eff}$ (m^2/s) are the molar fraction and effective Knudsen diffusion coefficient of species i; D_{ij}^{eff} (m^2/s) is the effective binary diffusion coefficient of species i and j; P(Pa) is total pressure; x is the depth measured from electrode surface; μ_m (Pa s) is viscosity of the gas mixtures; and B_0 is permeability of the porous anode.

Also, as is known:

$$
\sum_{i=1}^{n} y_i = 1 \tag{41}
$$

The diffusion process within a pore can be typically divided into two diffusion mechanisms: molecular diffusion and Knudsen diffusion. Molecular diffusion is dominant for large pore sizes and high system pressures while Knudsen diffusion becomes significant when the mean-free path of the molecular species is much larger than the pore size. $D_{i,k}^{eff}$ and D_{ij}^{eff} depend on the micro structure of the porous electrode (porosity, particle size, and tortuosity) and the operating conditions (temperature and pressure).

The model of charge transfer

The composite anode is porous structure which provides flow paths for reactants to and products from the anode TPBs. Besides, it also conducts electrons and ions through its solid portion, thereby providing flow paths for the transport of electrons and ions. So transport of electrons and ions in the solid portion of porous structure are modeled by applying conservation equations of charges. The conservation equations of charges can be expressed in terms of current density or potential. The governing equations are described as follows:

Electronic charge:

$$
\nabla\cdot i_e = R_a \tag{42}
$$

Ionic charge:

$$
\nabla\cdot i_i = -R_a \tag{43}
$$

Where i_e (A/m^2) and i_i (A/m^2) are electronic and ionic current density, respectively.

Expressing the electronic and ionic current density in terms of electronic and ionic potential through Ohm's law, we can obtain:

$$
\nabla\cdot\left(\sigma^{eff}\nabla\phi_e\right) = -R_a \tag{44}
$$

$$
\nabla\cdot\left(\kappa^{eff}\nabla\phi_i\right) = R_a \tag{45}
$$

Where ϕ_e (V) and ϕ_i (V) are electronic and ionic potential, respectively; σ^{eff} (S/m) and κ^{eff} (S/m) are the effective conductivities of electron- and ion-conducting materials in

Table 1 Governing equations in the composite anode

Governing equations	Composite anode
Species	$\nabla \cdot N_i = \dot{S}_{s,i}$
Dusty-gas model	$\frac{N_i}{D_{i,k}^{eff}} + \sum\limits_{j=1, j\neq i}^{n} \frac{y_i N_j - y_j N_i}{D_{ij}^{eff}} = -\frac{i}{RT}\left[P\frac{dy_i}{dx} + y_i \frac{dP}{dx}\left(1 + \frac{B_0 P}{D_{i,k}^{eff}\mu_m}\right)\right]$
Electronic charge	$\nabla \cdot i_e = R_a$ or $\nabla \cdot (\sigma^{eff}\nabla\varphi_e) = -R_a$
Ionic charge	$\nabla \cdot i_i = -R_a$ or $\nabla \cdot (\kappa^{eff}\nabla\varphi_i) = R_a$

composite anode, respectively. The effective electronic and ionic conductivity in composite anode are defined as:

$$\sigma^{eff} = \Phi\left(\frac{1-\varepsilon}{\tau}\right)\sigma \qquad (46)$$

$$\kappa^{eff} = (1-\Phi)\left(\frac{1-\varepsilon}{\tau}\right)\kappa \qquad (47)$$

Where σ (S/m) and κ (S/m) are the conductivities of pure electron- and ion-conducting materials (or the bulk electronic and ionic conductivities), respectively.

From above model description, the governing equations in composite anode are summarized in Table 1.

Definition of the coefficients

An empirical correlation [38] is used to obtain the binary diffusivity:

$$D_{ij} = 1.43 \times 10^{-7} \frac{T^{1.75}\left[\frac{1}{2}\left(\frac{1}{M_i} + \frac{1}{M_j}\right)\right]^{1/2}}{P\left[\nu_i^{1/3} + \nu_j^{1/3}\right]^2} \qquad (48)$$

Here ν_i and ν_j are the Fuller diffusion volume of two species given in Table 2.

The Knudsen diffusivity is commonly calculated based on literatures [31, 39, 40]:

$$D_{i,k} = \frac{d_{pore}}{3}\sqrt{\frac{8RT}{\pi M_i}} = 97\left(\frac{d_{pore}}{2}\right)\sqrt{\frac{T}{M_i}} \qquad (49)$$

The effective binary diffusivity is defined as:

$$D_{ij}^{eff} = \frac{\varepsilon}{\tau}D_{ij} \qquad (50)$$

In a similar manner, the effective Knudsen diffusivity can be written as:

$$D_{i,k}^{eff} = \frac{\varepsilon}{\tau}D_{i,k} \qquad (51)$$

The dynamic viscosity in multi-component systems at low pressure is described by Wilke's method [38]:

$$\mu_m = \sum\limits_{i=1}^{n} \frac{y_i \mu_i^0}{\sum\limits_{j=1}^{n} y_j \phi_{ij}} \qquad (52)$$

$$\phi_{ij} = \frac{\left[1 + \left(\mu_i^0/\mu_j^0\right)^{1/2}\left(M_j/M_i\right)^{1/4}\right]^2}{\left[8\left(1 + \left(M_i/M_j\right)^{1/2}\right)\right]} \qquad (53)$$

For the dynamic viscosity of a pure component, a six-order polynomial correlation from literature [38] is used:

$$\mu_i^0 = \sum\limits_{k=0}^{6} b_k \theta^k \qquad (54)$$

Where $\theta = \frac{T}{1000K}$, μ_i^0 in the unit of $\mu\text{Poise} = 10^{-7}$ Pa s.

B_0 is the permeability of the porous electrode in Eq. 37, which can be calculated by the Kozeny–Carman relationship [41]:

Table 2 The thermal properties data [38]

Species	Molar mass (gmol^{-1})	Fuller et al. diffusion volume	b_0	b_1	b_2	b_3	b_4	b_5	b_6
CH$_4$	16.04	25.14	−9.9989	529.37	−543.82	548.11	−367.06	140.48	−22.92
CO	28.01	18.0	−4.9137	793.65	−875.9	883.75	−572.14	208.42	−32.298
H$_2$O	18.01	13.1	−6.7541	244.93	419.5	−522.38	348.12	−126.96	19.591
H$_2$	2.016	6.12	15.553	299.78	−244.34	249.41	−167.51	62.966	−9.9892
CO$_2$	44.01	26.7	−20.434	680.07	−432.49	244.22	−85.929	14.45	−0.4564

Table 3 Fuel composition at the anode surface for the model validation

Species	Molar fraction
CH_4	0.171
H_2	0.263
H_2O	0.493
CO	0.029
CO_2	0.044

$$B_0 = \frac{\varepsilon^3}{72\tau(1-\varepsilon)^2}(2d_{pore})^2 \qquad (55)$$

Boundary conditions

For computing mathematical formulation of SOFC anode micro model, the boundary conditions at anode surface where $x=0$ and the interface between anode and electrolyte where $x=l_a$ are needed. At $x=0$, the boundary condition is a defined boundary condition where the composition of species is specified, the pressure is barometric pressure, ionic current density is zero, and electronic current density is equal to total current density. At $x=l_a$, the molar flux and electronic current density are zero and ionic current density is equal to total current density. In term of mathematical form, the boundary conditions are given as:

$$x = 0 : y_i = \text{ species}; i_e = \text{i}; i_i = 0; P = 101325 \text{ Pa}$$

$$x = l_a : N_i = 0; i_e = 0; i_i = \text{i}$$

The validation of the model

The solution obtained from the developed model is compared with the one-dimensional numerical solution for multi-component diffusion inside the porous SOFC anode provided by Haberman and Young [36]. The parameters obtained from Haberman and Young's model are listed in Tables 3 and 4. In the model of Haberman and Young [36], the Knudsen diffusion was ignored and the electrochemical reaction was assumed to occur exclusively at the interface between anode and electrolyte. Besides, there were no chemical reactions in the porous anode. For comparing the solution obtained from the present model with the solution of Haberman and Young's model, the present model is changed accordingly.

Figure 4 shows the distribution of species inside porous anode at 3 A cm^{-2}. Obviously, the results obtained from present model are in good agreement with numerical solution from the model of Haberman and Young [36]. Therefore, it is reasonable to use the developed model to study the characteristic of SOFC and predict the cell performance.

Results and discussions

The established model can be used to investigate the effect of pressure gradient on electrochemical characteristics of composite anode. The basic parameters and fuel composition used in the present mathematical model are listed in Tables 3 and 5. Most of the parameters used in the model are representative values reported in literatures [26, 27, 37, 38, 41–44]. Here,
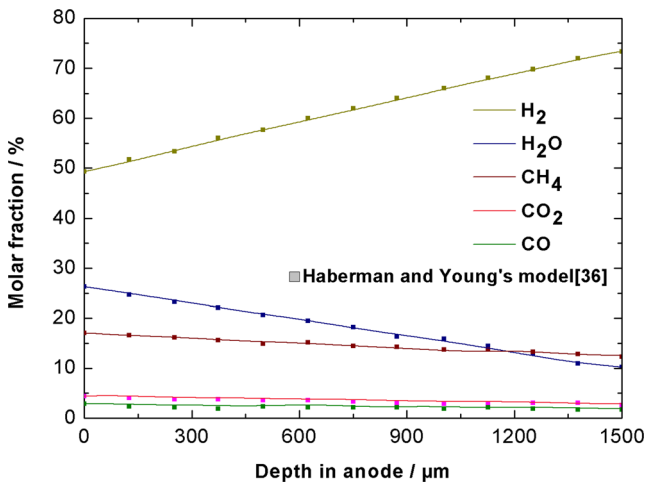
Table 4 Parameters used in the model validation

Parameters	Value
Operating temperature, T	1,123 K
Total pressure at the anode surface, P	1.0 atm
Anode thickness, l_a	1,500 μm
Porosity, ε	0.3 [38]
Tortuosity, τ	4.5 [43, 44]
Pore diameter, d_{pore}	1.0 μm [42]
Contact angle between the electron and ion-conducting particles, θ	15^0 [37]
Radius of the electron-conducting particles, r_{el}	0.1 μm [26, 38]
Radius of the ionic-conducting particles, r_{io}	0.1 μm [26, 38]
Volume fraction of the electron-conducting particles, Φ	0.5 [27, 38]
Reference H_2 concentration, $c_{H_2,ref}$	10.78 mol m^{-3}
Reference exchange current density for H_2 oxidation, $i_{0,ref}^{H_2}$	1,320 A m^{-2} [42]
Reaction order for H_2 oxidation, γ_{H_2}	0.5
Resistivity of the electron-conducting particles, ρ_{el}	$2.98 \times 10^{-5}\exp\left(-\frac{1332}{T}\right)$ Ωm [41]
Resistivity of the ion-conducting particles, ρ_{io}	$2.94 \times 10^{-5}\exp\left(-\frac{10325}{T}\right)$ Ωm [41]
Total current density, i	30000 A m^{-2}

Fig. 4 Distribution of molar fractions of species through the porous anode (The *lines* represent the molar fractions of the species predicted by the present model, and the *symbol* represents the solution obtained from Haberman and Young's model)

total pressure at the anode surface and the operating temperature are set as 1 atm and 1,073 K, respectively.tgroup

Figure 5 shows the distribution of pressure in composite anode. The pressure in the composite anode is found to increase observably along the depth of composite anode. From Fig. 5, it can be seen that the pressure at the interface between the anode and electrolyte where $x = l_a$ is 127,599 Pa, about 25.93 % higher than the pressure at the anode surface where $x = 0$. The phenomenon can be explained by two reasons. On the one hand, from Eqs. 1 to 3, the molar number of MSR products is twice as many as that of reactants, while the molar number of WGS products is equal to that of the reactants. Meanwhile, during the electrochemical oxidation reaction,

one molar H_2 can produce one molar H_2O. So, the total molar number of MSR, WGS, and electrochemical reaction products is larger than that of reactants. On the other hand, the diffusion of H_2O is more difficult than H_2 due to its larger molecular weight [45]. Since the pressure increases along the composite anode, it means that the pressure gradient exists in the anode. Thus, it is necessary to think about the pressure gradient in the anode micro modeling. In the following, the influence of pressure gradient on electrochemical characteristics of composite anode will be discussed. Therefore, two cases are presented. One is the mass transfer is described by DGM considering pressure gradient, which is formulated in Eq. 37; another one is the mass transfer is described by DGM without pressure gradient, which is represented by Eq. 38.

Figure 6 shows the molar fractions of H_2 and H_2O, respectively. Obviously, Fig. 6a shows the molar fraction of H_2 is lower if the pressure gradient is considered and Fig. 6b shows the molar fraction of H_2O is larger than the case neglecting the pressure gradient. This is because of the fact that the pressure gradient hinders the transport of H_2 and favors the transport of H_2O. The two figures also show that the difference of molar fraction between the case considering pressure gradient and the case neglecting pressure gradient increases along the anode depth. The molar fraction of H_2 considering pressure gradient is about 21.43 % lower than that without pressure gradient at the interface between the anode and electrolyte; the molar fraction of H_2O considering pressure gradient is about 18.16 % higher than that without pressure gradient at the interface between the anode and electrolyte.

Figure 7 shows the distribution of molar fractions of CO, CO_2, and CH_4 in the composite anode. It can be concluded that the molar fractions of CO and CO_2 are lower than the case

Table 5 Parameters used in the present mathematical model

| Parameters	Value
Operating temperature, T	1,073 K
Total pressure at the anode surface, P	1.0 atm
Anode thickness, l_a	500 μm
Porosity, ε	0.3 [38]
Tortuosity, τ	4.5 [43, 44]
Pore diameter, d_{pore}	1.0 μm [42]
Contact angle between the electron- and ion-conducting particles, θ	15^0 [37]
Radius of the electron-conducting particles, r_{el}	0.1 μm [26, 38]
Radius of the ionic-conducting particles, r_{io}	0.1 μm [26, 38]
Volume fraction of the electron-conducting particles, Φ	0.5 [27, 38]
Reference H_2 concentration, $c_{H_2,ref}$	10.78 mol m^{-3}
Reference exchange current density for H_2 oxidation, $i_{0,ref}^{H_2}$	1,320 A m^{-2} [42]
Reaction order for H_2 oxidation, γ_{H_2}	0.5
Resistivity of the electron-conducting particles, ρ_{el}	$2.98 \times 10^{-5} \exp\left(-\frac{1332}{T}\right)$ Ωm [41]
Resistivity of the ion-conducting particles, ρ_{io}	$2.94 \times 10^{-5} \exp\left(-\frac{10325}{T}\right)$ Ωm [41]
Total current density, i	5,000 A m^{-2}
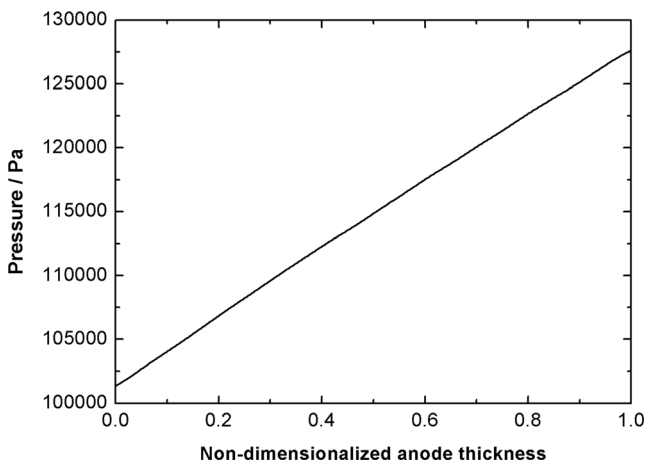
Fig. 5 Distribution of pressure in the composite anode

considering the pressure gradient, while the molar fraction of CH_4 is higher than the case which the pressure gradient is taken into account. The results obtained are because the pressure gradient favors the transport of CO, CO_2, and H_2O and
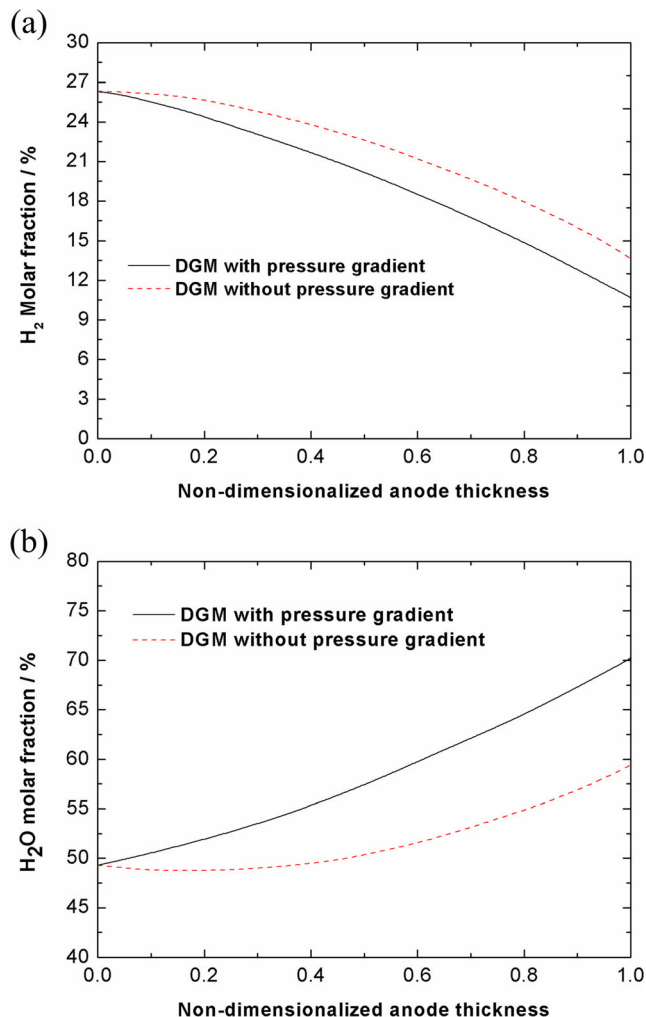

Fig. 6 Distributions of molar fractions of H_2 and H_2O in the composite anode: a molar fraction of H_2 and b molar fraction of H_2O
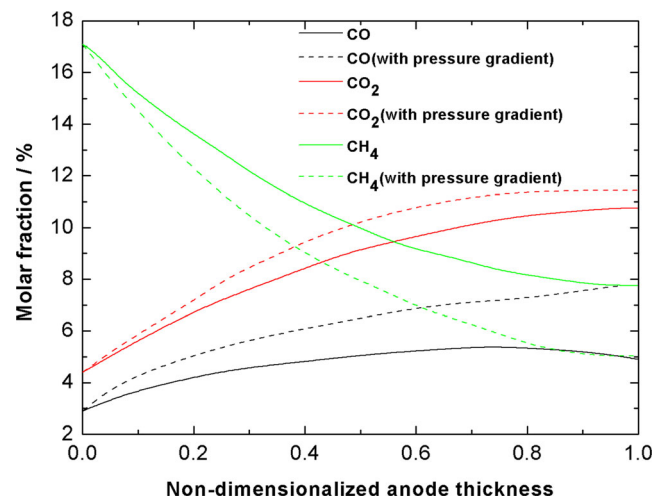

Fig. 7 Distribution of molar fractions of CO, CO_2, and CH_4 in the composite anode

impedes the transport of H_2 and CH_4, in addition to this, the result also caused by the interactions of chemical reactions, electrochemical reaction, mass transfer, and charger transfer. It also can be seen that the difference of molar fraction of each component between two cases increases along the anode depth, except for the difference of molar fraction of CO_2.

Figure 8 shows the MSR reaction rate in the composite anode. From Fig. 6, when the pressure gradient is considered, the results show that there is larger H_2O molar fraction and smaller H_2 molar fraction, thus higher rate of MSR can be revealed in Fig. 8. From the curves in Fig. 8, it can be seen that the rate of MSR decreases along the depth of anode initially and increases in anode near the interface between the anode and electrolyte. The reason why the phenomenon appeared is that the molar fraction of CH_4 is decreased and the molar fraction of H_2O is increased. The decrease in H_2 molar fraction and augment in H_2O molar fraction result in the increase of the rate of MSR, then bring about the increase of pressure gradient in the composite anode in turn, because only MSR can change the pressure in the composite anode.

Figure 9 shows the distributions of non-dimensionalized electronic and ionic current density in the composite anode, respectively. From the distributions of electronic and ionic current density, it can be seen that electronic and ionic current density remain constant for most of the length of the anode before starting to vary at the end of the anode thickness. It is concluded that the pressure gradient has no obvious impacts on the electronic and ionic current densities within a distance which from the anode surface. However, it will affect the electronic current density and ionic current density obviously at the end of anode thickness. The electronic current density and ionic current density in the anode have been discussed in two cases. One case is the DGM neglecting the pressure gradient, the other case is the DGM considering the pressure gradient. The difference between the two cases reaches the
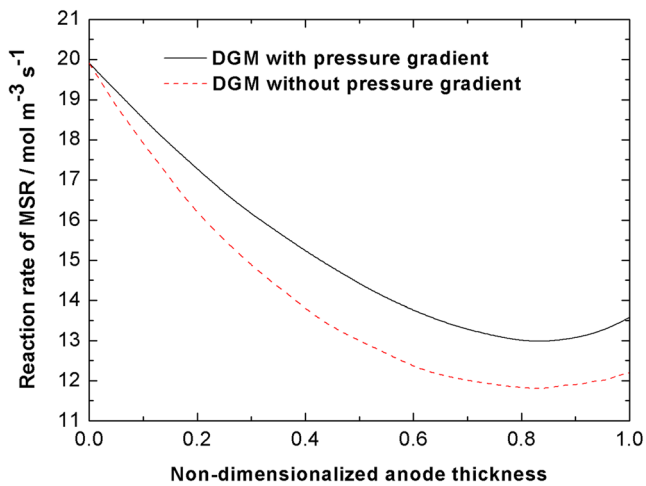
Fig. 8 Distribution of MSR reaction rate in the composite anode
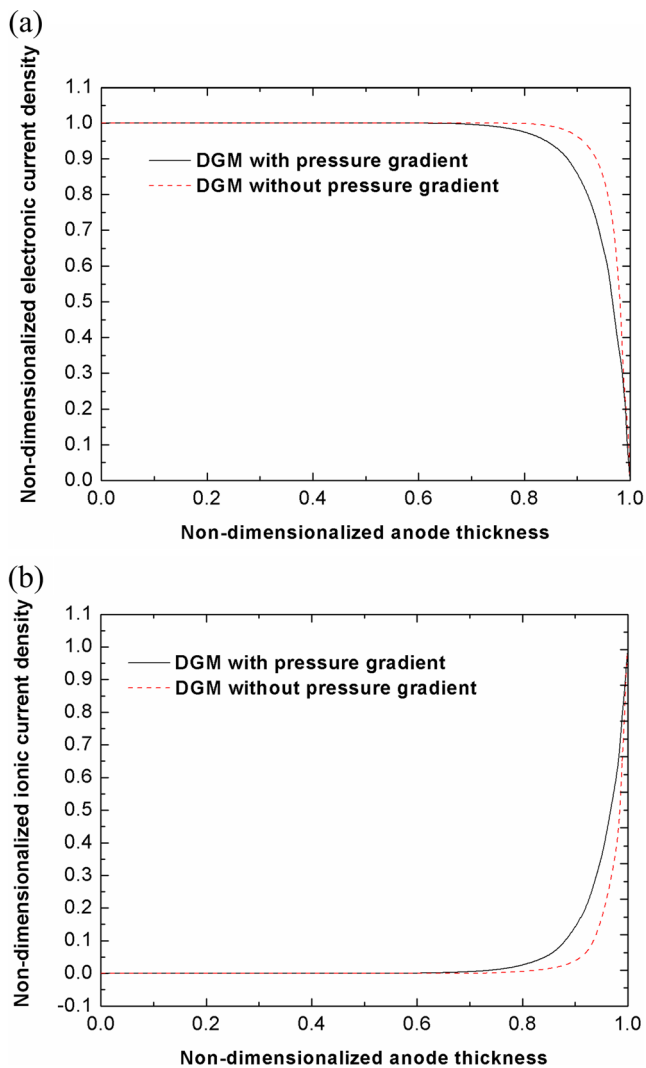
(a)

(b)

Fig. 9 Distributions of non-dimensionalized electronic and ionic current density in the composite anode: **a** electronic current density and **b** ionic current density

maximum at the distance about 91 % from the anode surface. The electronic current density considering pressure gradient is about 14.58 % lower than the case without pressure gradient at the distance about 91 % from the anode surface; the ionic current density considering pressure gradient is about 14.58 % higher than the case without pressure gradient at the distance about 91 % from the anode surface. The results from Fig. 9a, b verify the concept of treating an SOFC electrode as two finite layers which consist of electrode backing layer that consists of electron-conducting particles only and reaction zone layer that consists of electron- and ion-conducting particles [11]. It means most electrochemical reaction sites local at the reaction zone layer.

Similarly, the distributions of electronic and ionic potential are shown in Fig. 10. It has the same trend with the distributions of electronic and ionic current density. The curves also can verify the point of treating a SOFC electrode as two finite layers and show that the pressure gradient only can affect a small portion of the anode evidently. Due to anode activation overpotential η_a can be expressed by $\phi_i - \phi_e$, and the electronic
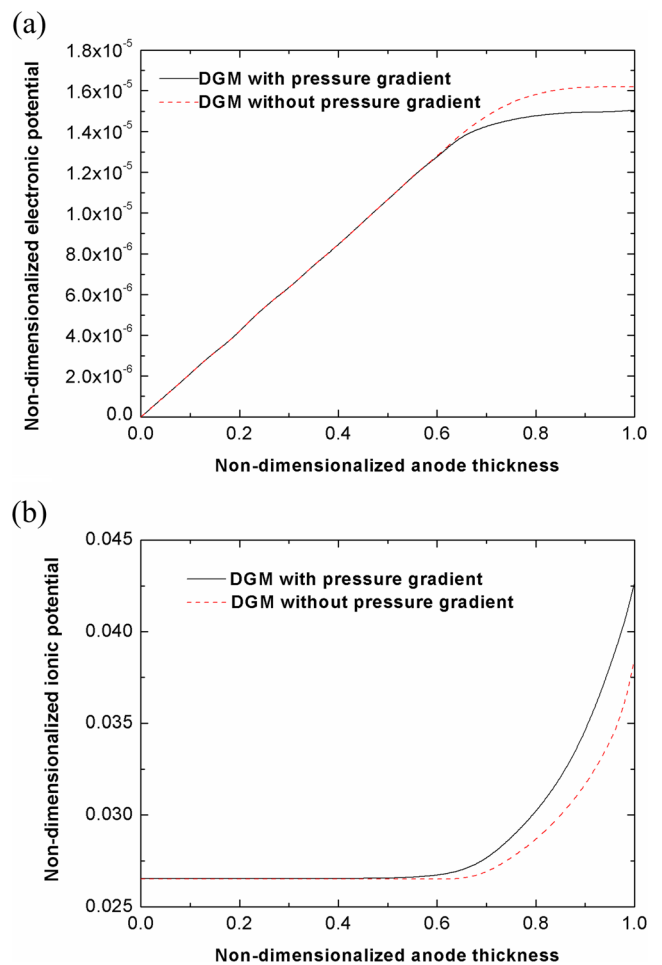
(a)

(b)

Fig. 10 Distributions of non-dimensionalized electronic and ionic potential in the composite anode: **a** electronic potential and **b** ionic potential
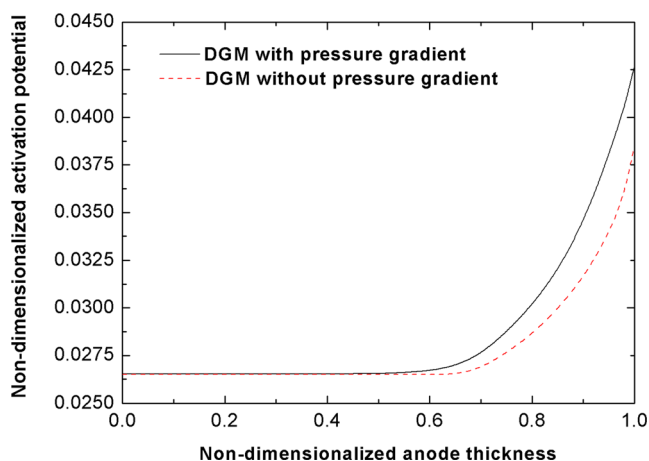
Fig. 11 Distribution of non-dimensionalized activation potential in the composite anode

and ionic potential are different under the two cases, then the anode activation overpotential is different. Under the influence of pressure gradient, the electronic potential is lower and the ionic potential is higher. So the anode activation overpotential is increased, which can be described in Fig. 11. At last, it can draw a conclusion that the anode activation overpotential can be affected by pressure gradient. From above curves, we can see that the pressure gradient only affects the reaction zone layer obviously, while has little influence on the electrode layer. This is because the ionic conductivity of ion-conducting particle is low, which restricts the transport of oxide ions through the anode and then limits the thickness of reaction zone layer. It means the number of active TPB in electrode layer is smaller than that in reaction zone layer.

In the end, it can be concluded that the pressure gradient has a great effect in anode micro modeling of a SOFC running on hydrocarbon fuels with internal reforming and water gas shift, especially in the reaction zone layer.

Conclusions

A theoretical mathematical model has been constructed to study the role of pressure gradient in anode micro modeling of SOFC. The SOFC anode is modeled as porous composite structure composed by electronic and ionic conducting particles where electrochemical reactions are considered to occur throughout the anode, according with the micro modeling approach of treating electrodes. The results show that the pressure increases along the anode depth. From the molar fraction distributions of H_2, H_2O, CO, CO_2, and CH_4, it is known that the molar fractions of H_2 and CH_4 are lower if the pressure gradient is considered; the molar fractions of H_2O, CO, and CO_2 are larger than the case of neglecting the pressure gradient. The results show that the composite anode can be

regarded as two parts, consists of electrode backing layer and reaction zone layer, then verify the point of treating an SOFC electrode as two finite layers exactly [11]. The pressure gradient has no significant effect on electrode backing layer and can influence the electronic and ionic current density greatly in reaction zone layer. The model also can obtain the electronic potential and ionic potential under the case of considering pressure gradient and the case that neglects the pressure gradient, the difference of the characteristics of anode between the two cases can be found. It means the anode activation overpotential, and then anode overpotential is different if the pressure gradient is considered. So, the model can be used to predict the characteristics of SOFC further. The model proposed only discusses the effect of pressure gradient on the anode micro modeling of SOFC. Therefore, the model developed can predict the characteristics of anode more accurately and then help to improve the performance of SOFC.

References

1. Gorte RJ (2005) Recent developments towards commercialization of solid oxide fuel cells. AIChE J 51(9):2377–2381. doi:10.1002/aic.10621
2. Recknagle KP, Williford RE, Chick LA, Rector DR, Khaleel MA (2003) Three-dimensional thermo-fluid electrochemical modeling of planar SOFC stacks. J Power Sources 113(1):109–114. doi:10.1016/s0378-7753(02)00487-1
3. Khaleel MA, Lin Z, Singh P, Surdoval W, Collin D (2004) A finite element analysis modeling tool for solid oxide fuel cell development: coupled electrochemistry, thermal and flow analysis in MARC®. J Power Sources 130(1–2):136–148. doi:10.1016/j.jpowsour.2003.11.074
4. Singhal SC (2002) Solid oxide fuel cells for stationary, mobile, and military applications. Solid State Ionics 152–153:405–410. doi:10.1016/s0167-2738(02)00349-1
5. Chan SH, Xia ZT (2002) Polarization effects in electrolyte/electrode-supported solid oxide fuel cells. J Appl Electrochem 32(3):339–347
6. Chan SH, Khor KA, Xia ZT (2001) A complete polarization model of a solid oxide fuel cell and its sensitivity to the change of cell component thickness. J Power Sources 93(1–2):130–140
7. Ni M, Leung M, Leung DC (2006) A modeling study on concentration overpotentials of a reversible solid oxide fuel cell. J Power Sources 163(1):460–466
8. Ni M, Leung M, Leung D (2007) Parametric study of solid oxide fuel cell performance. Energy Convers Manag 48(5):1525–1535
9. Jamsak W, Assabumrungrat S, Douglas PL, Croiset E, Laosiripojana N, Suwanwarangkul R, Charojrochkul S (2007) Thermodynamic assessment of solid oxide fuel cell system integrated with bioethanol purification unit. J Power Sources 174(1):191–198. doi:10.1016/j.jpowsour.2007.08.105
10. Ishihara T, Tabuchi J, Ishikawa S, Yan J, Enoki M, Matsumoto H (2006) Recent progress in LaGaO3 based solid electrolyte for

intermediate temperature SOFCs. Solid State Ionics 177(19–25): 1949–1953. doi:10.1016/j.ssi.2006.01.044

11. Hussain MM, Li X, Dincer I (2009) A numerical investigation of modeling an SOFC electrode as two finite layers. Int J Hydrog Energy 34(7):3134–3144

12. Ni M (2010) 2D thermal-fluid modeling and parametric analysis of a planar solid oxide fuel cell. Energy Convers Manag 51(4):714–721

13. Ni M (2013) The effect of electrolyte type on performance of solid oxide fuel cells running on hydrocarbon fuels. Int J Hydrog Energy 38(6):2846–2858

14. Ni M (2010) Modeling of a planar solid oxide fuel cell based on proton-conducting electrolyte. Int J Energy Res 34(12):1027–1041

15. Hussain MM, Li X, Dincer I (2006) Mathematical modeling of planar solid oxide fuel cells. J Power Sources 161(2):1012–1022. doi:10.1016/j.jpowsour.2006.05.055

16. Ni M, Leung DYC, Leung MKH (2008) Importance of pressure gradient in solid oxide fuel cell electrodes for modeling study. J Power Sources 183(2):668–673. doi:10.1016/j.jpowsour.2008.05.013

17. Hussain MM, Li X, Dincer I (2005) Multi-component mathematical model of solid oxide fuel cell anode. Int J Energy Res 29(12):1083–1101. doi:10.1002/er.1141

18. Tang CQ, Liu L, Qian XL, Guo X, Sun YQ, Yao KL, Cui K (1998) Overview on grain-boundary and transport problems in solid oxide fuel cell. Ionics 4(5–6):472–476. doi:10.1007/BF02375892

19. Mirahmadi A, Valefi K (2011) Study of thermal effects on the performance of micro-tubular solid-oxide fuel cells. Ionics 17(9):767–783. doi:10.1007/s11581-011-0559-x

20. Dhaouadi H, Fadhalaoui A, Mdani A, Rzaigui M (2014) Structural and electrical properties of nanostructured cerium phosphate. Ionics 20(6):857–866. doi:10.1007/s11581-013-1045-4

21. Bokalawela RSP, Dissanayake MAKL, Mellander BE, Albinson I (2004) H2/Pt/Ce0.9Gd0.1O1.95/Pt/O2 fuel cell operated in the intermediate temperature range 500–700 °C. Ionics 10(1–2):84–87. doi:10.1007/BF02410311

22. Clague R, Shearing PR, Lee PD, Zhang Z, Brett DJL, Marquis AJ, Brandon NP (2011) Stress analysis of solid oxide fuel cell anode microstructure reconstructed from focused ion beam tomography. J Power Sources 196(21):9018–9021. doi:10.1016/j.jpowsour.2010.12.097

23. Celik S, Ibrahimoglu B, Toros S, Mat MD (2014) Three dimensional stress analysis of solid oxide fuel cell anode micro structure. Int J Hydrog Energy 39(33):19119–19131. doi:10.1016/j.ijhydene.2014.09.110

24. Celik S, Ibrahimoglu B, Mat MD, Kaplan Y, Veziroglu TN Micro level two dimensional stress and thermal analysis anode/electrolyte interface of a solid oxide fuel cell. International Journal of Hydrogen Energy (0). doi:http://dx.doi.org/10.1016/j.ijhydene.2014.10.057

25. Costamagna P, Costa P, Antonucci V (1998) Micro-modelling of solid oxide fuel cell electrodes. Electrochim Acta 43(3–4):375–394

26. Chen XJ, Chan SH, Khor KA (2004) Simulation of a composite cathode in solid oxide fuel cells. Electrochim Acta 49(11):1851–1861

27. Deseure J, Bultel Y, Dessemond L, Siebert E (2005) Theoretical optimisation of a SOFC composite cathode. Electrochim Acta 50(10):2037–2046

28. Ni M, Leung MKH, Leung DYC (2007) Micro-scale modelling of solid oxide fuel cells with micro-structurally graded electrodes. J Power Sources 168(2):369–378. doi:10.1016/j.jpowsour.2007.03.005

29. Hussain MM, Li X, Dincer I (2009) A general electrolyte-electrode-assembly model for the performance characteristics of planar anode-supported solid oxide fuel cells. J Power Sources 189(2):916–928

30. Hussain MM, Li X, Dincer I (2007) Mathematical modeling of transport phenomena in porous SOFC anodes. Int J Therm Sci 46(1):48–56

31. Suwanwarangkul R, Croiset E, Fowler MW, Douglas PL, Entchev E, Douglas MA (2003) Performance comparison of Fick's, dusty-gas and Stefan-Maxwell models to predict the concentration overpotential of a SOFC anode. J Power Sources 122(1):9–18

32. Matsuzaki Y, Yasuda I (2000) Electrochemical Oxidation of H 2 and CO in a H 2 - H 2 O - CO - CO 2 System at the Interface of a Ni-YSZ Cermet Electrode and YSZ Electrolyte. J Electrochem Soc 147(5): 1630–1635

33. Janardhanan VM, Deutschmann O (2007) Numerical study of mass and heat transport in solid-oxide fuel cells running on humidified methane. Chemical Engineering Science19th International Symposium on Chemical Reaction Engineering - From Science to Innovative Engineering ISCRE-19 62 (18–20):5473–5486. doi:10.1016/j.ces.2007.01.043

34. Mogensen D, Grunwaldt JD, Hendriksen PV, Dam-Johansen K, Nielsen JU (2011) Internal steam reforming in solid oxide fuel cells: status and opportunities of kinetic studies and their impact on modelling. J Power Sources 196(1):25–38. doi:10.1016/j.jpowsour.2010.06.091

35. Lehnert W, Meusinger J, Thom F (2000) Modelling of gas transport phenomena in SOFC anodes. J Power Sources 87(1–2):57–63

36. Haberman BA, Young JB (2004) Three-dimensional simulation of chemically reacting gas flows in the porous support structure of an integrated-planar solid oxide fuel cell. Int J Heat Mass Transfer 47(17–18):3617–3629

37. Sunde S (2000) Simulations of composite electrodes in fuel cells. J Electroceram 5(2):153–182

38. Todd B, Young JB (2002) Thermodynamic and transport properties of gases for use in solid oxide fuel cell modelling. J Power Sources 110(1):186–200

39. Zhu H, Kee RJ (2003) A general mathematical model for analyzing the performance of fuel-cell membrane-electrode assemblies. J Power Sources 117(1–2):61–74. doi:10.1016/s0378-7753(03)00358-6

40. Jeon DH (2009) A comprehensive CFD model of anode-supported solid oxide fuel cells. Electrochim Acta 54(10):2727–2736. doi:10.1016/j.electacta.2008.11.048

41. Ni M, Leung MKH, Leung DYC (2007) Mathematical modeling of the coupled transport and electrochemical reactions in solid oxide steam electrolyzer for hydrogen production. Electrochim Acta 52(24):6707–6718. doi:10.1016/j.electacta.2007.04.084

42. Kim JW, Virkar AV, Fung KZ, Mehta K, Singhal SC (1999) Polarization effects in intermediate temperature, anode-supported solid oxide fuel cells. J Electrochem Soc 146(1):69–78

43. Yakabe H, Hishinuma M, Uratani M, Matsuzaki Y, Yasuda I (2000) Evaluation and modeling of performance of anode-supported solid oxide fuel cell. J Power Sources 86(1–2):423–431

44. Williford RE, Chick LA (2003) Surface diffusion and concentration polarization on oxide-supported metal electrocatalyst particles. Surf Sci 547(3):421–437

45. Schmidt VH, Tsai C-L (2008) Anode-pore tortuosity in solid oxide fuel cells found from gas and current flow rates. J Power Sources 180(1):253–264. doi:10.1016/j.jpowsour.2008.01.073